The Effect of Shock Heating on the Stability of Laser-Driven Targets

Introduction

Hydrodynamic instability is a key issue for inertial confinement fusion (ICF).[1–3] The effects of the Rayleigh–Taylor (RT) instability can be reduced by shocks that heat the target shell, causing a slight decompression; this increases the ablation velocity and reduces the RT growth rate.[4,5] ICF target designs use shock heating to determine the implosion isentrope to establish a balance between performance and stability. This article presents the first experimental demonstration of a correlation between increased hydrodynamic stability and higher shock temperatures produced early in the interaction. This correlation is attributed to increased ablative stabilization resulting from target decompression caused by shock heating.

Experimental Implementation

Pulse shapes with different rise times were used to irradiate planar CH targets that had embedded Al layers whose temperatures were probed using time-resolved x-ray absorption spectroscopy. The 1*s*–2*p* Al absorption lines provided information about the ionization state of the Al, which, in turn, was used to infer both the shock-induced temperature and the heat-front propagation into the targets. The experiments indicate that steeply rising drive pulses produce shocks that heat the embedded Al layer to ~25 eV, while the slowly rising pulses produce shock heating below ~15 eV—our detection threshold. The heat front driven by the rapidly rising pulses showed the expected behavior, whereas the slowly rising pulses experienced mixing[6] caused by the RT instability that is seeded by laser imprinting.[7] Mix was not observed in the rapid-rise pulses because increased shock heating produces higher ablative stabilization.

In these experiments, 20-μm-thick CH targets were irradiated by six UV OMEGA[8] beams having 0.2-THz smoothing by spectral dispersion (SSD).[9] A 0.5-μm-thick layer of Al was embedded at either 5 or 10 μm below the irradiated surface. The laser pulses were either (1) a steeply rising (~200-ps rise time), nearly square shaped pulse with 1-ns duration and on-target intensity of $\sim 4 \times 10^{14}$ W/cm^2 or (2) a "ramp" pulse that rose linearly to 3×10^{14} W/cm^2 in 3 ns. One-dimensional calculations indicate that these pulses produce shock pressures of ~35 Mb and ~15 Mb, respectively. The targets were probed with x rays from a microdot of Sm that were dispersed by a streaked x-ray spectrometer.

Observations

Figure 85.6(a) shows the time-resolved absorption spectrum from a 20-μm-thick CH target (with the Al layer 10 μm deep) irradiated with the square pulse. Along the spectral direction, the 1*s*–2*p* absorption lines (dark bands) due to ionization states from F-like Al to Li-like Al are identified. The detailed structure of these transition arrays is not re-

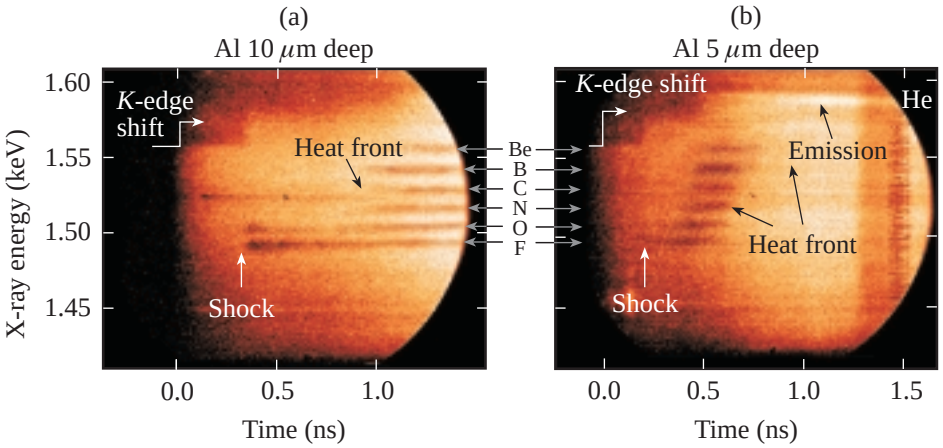

S18244, S18243
E10346

Figure 85.6
(a) Time-resolved absorption spectrum (dark horizontal bands) from an Al layer embedded 10 μm deep in a 20-μm-CH target irradiated by a square pulse. The F- and O-like absorption lines appear at ~325 ps due to shock heating. Later (~800 ps), higher ionization states occur when the heat front reaches the Al. (b) Absorption spectrum with the Al layer 5 μm deep. The F- and O-like absorption lines appear at ~200 ps and the heat front arrives at ~400 ps. He-like Al *emission* is observed when the heat front reaches the Al.

solved, but their mean energies and widths are consistent with predictions[10] and other observations.[11] The data in Fig. 85.6(a) indicate that both F-like and O-like lines appear at ~325 ps, and then later at ~800 ps, higher ionization states appear in progression.

Time is referenced to the start of the drive pulse that is preceded 300 ps by the backlighter. This allows observation of the *K*-shell absorption edge (at ~1.56 keV) in *cold* Al. At approximately the same time that the F-like and O-like lines appear, the *K* edge shifts to higher energy. This results primarily from the change in ionization of the Al ions. Later, as higher ionization states (N-like and above) appear, the *K* edge shifts to higher energy.

The abrupt onset of the F-like and O-like absorption lines is caused by shock heating of the Al layer; the higher ionization states (that appear later at a time ~800 ps) result from the incipient heating by the laser-driven heat front. These dynamics are confirmed by data from a target with the Al layer closer to the surface. Figure 85.6(b) is the spectrum from an experiment with the Al layer 5 μm deep. Here the onset of the F-like and O-like Al absorption lines is not clear, but one can readily see the abrupt change in the *K*-edge energy occurring at ~200 ps, consistent with the shock speed inferred from Fig. 85.6(a). Here the heat front also arrives earlier (~400 ps), but, in this case, the heating is sufficient to not only create absorption in higher ionization states but also produce He-like *emission*. The He-like emission occurs because the heat front has penetrated the 5 μm CH, and has then heated and ablated the Al. The absorption lines are short lived because the temperature rises sufficiently to "burn through" these states, thereby reducing the population in the lower tail of the charge-state distribution.

The dependence of shock heating on the temporal profile of the drive was measured by irradiating similar targets with the ramp pulse. Figure 85.7 shows an extended temporal record of absorption spectra from a target having the Al layer 5 μm deep and irradiated by the ramp pulse. The backlighter produces bright, broadband emission that ceases at ~2 ns. Coincidentally at that time He-like Al emission begins, which indicates that portions of the Al are heated to over 500 eV. Preceding this emission, no Al absorption lines (1.48 to 1.56 keV) are observed. Similar experiments on targets with the Al 10 μm deep also showed no absorption lines on these shots; the He-like emission occurred ~400 ps later than that shown in Fig. 85.7. These results are significant for two reasons: (1) They indicate the absence of significant shock heating before emission begins. (Note, however, that the *K* edge at 1.56 keV becomes diffuse at about 600 ps, suggesting some low-level shock heating.) (2) The lack of absorption lines preceding the He-like emission suggests that Al is instantaneously heated from <15 eV to >500 eV, contrary to expected behavior. Heat fronts in both directly driven[12] and indirectly driven targets[11] normally exhibit a succession of Al absorption lines that appear before the emission lines, as in Fig. 85.6(b).

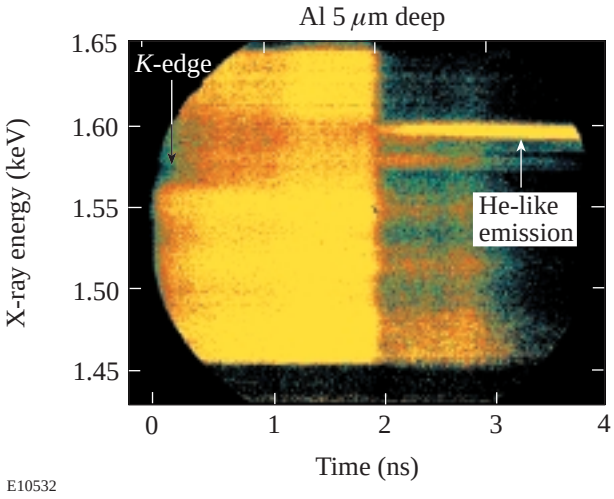

Figure 85.7
Absorption spectra from a target with the Al layer 5 μm deep and irradiated by a ramp pulse. No Al absorption lines are observed preceding the Al He-like emission lines that begin at ~1.9 ns.

In summary, the slowly rising ramp pulse produces less shock heating (no absorption lines) than the square pulse, and targets driven by the ramp pulse show no Al absorption lines even in the presence of He-like emission. The latter observation will be attributed to the effects of RT instability, while the former will confirm the correlation of ablative stabilization with shock heating.

Analysis and Discussion

The relative populations of Al charge states and the resulting absorption spectra were calculated for steady-state conditions at various temperatures.[13] This allowed the Al temperature to be inferred as a function of time. Figure 85.8 shows the Al temperature measured (points) and predicted (curves) by 1-D simulations (*LILAC*[14]). Figure 85.8(a) compares calculations and measurements for square-pulse irradiation of targets with the Al layer 5 μm deep (solid line and circles) and 10 μm deep (dashed line and triangles). Both the shock heating of the Al to ~25 eV and the heat-front penetration ($\gtrsim$40 eV) are correctly predicted by the 1-D simulations, indicating stable

target behavior. The minor discrepancy in timing of the heat-front arrival times is likely the result of 2-D effects (see below). The lower limit for this measurement technique is the onset of F-like absorption lines that occurs at about 15 eV. The error bars indicate a ±100-ps timing uncertainty in the camera and a ±10-eV precision of the temperature measurement.

Similar temperature profiles for the ramp pulse are shown in Fig. 85.8(b) [5 μm deep (solid/circles); 10 μm deep (dashed/triangles)]. Since there were no absorption lines in the data, only the onset times for Al emission (defined as 500 eV) are shown. The predicted temperatures are below the ~15-eV experimental detection threshold until about 1.7 ns, when the heat front arrives at the Al, which reaches ~500 eV at 1.9 ns for the 5-μm case. The 10-μm case is not predicted to be heated above ~40 eV, yet the experiment reaches 500 eV at ~2.3 ns. The temperature rise predicted (by a 1-D code) for the ramp pulse is similar to that for the square pulse [Fig. 85.8(a)], indicating that the lack of absorption lines is not due to a steep temperature rise.

To explain the observation that the heat front reaches the 10-μm-deep Al layer and the He-like emission occurs with no preceding Al absorption lines, the existence of a mixing region is postulated. The emission lines could result from Al that is prematurely mixed into the ablation region.[6] Using the model discussed in Ref. 15, the thickness of that mix layer was calculated and then added to the depth predicted by 1-D simulations. The mix layer is produced by the RT instability that amplifies imprinted perturbations,[7] producing considerable two-dimensional effects. The model uses the measured spectrum of irradiation nonuniformities to calculate the imprinted perturbations, and then calculates their growth[16] and saturation.[17] The curves in Fig. 85.9 show the calculated location of the ablation surface (the point of steepest density gradient) in uncompressed CH thickness for the square and ramp pulses. The heavy lines are the predictions of 1-D calculations, and the shaded regions are the calculated mix layers centered on those predictions. The data represent the times when the Al layer (buried at the plotted depth) begins to produce He-like emission. Once ablated, this material must traverse the conduction zone before it is heated in the corona. The square-pulse data are not significantly affected by the RT instability and are therefore reasonably predicted by 1-D simulations. In contrast, the ramp pulse has a mix layer that affects the apparent penetration at both 5- and 10-μm depths in the original target. [The temporal offset (~250 ps) between the data and simulations corresponds to the time for the Al to travel from the ablation surface to the 500-eV isotherm.[18]] This explains both the unexpected emission from the Al [10-μm result in Fig. 85.8(b)] and the lack of preceding absorption lines for the 5- and 10-μm cases. Specifically, the RT spikes can "leach" Al from the embedded layer out into the corona (where it emits), whereas the Al in the bubbles has not been heated significantly and therefore has no absorption signature. The relative size of the bubbles and spikes is such that the bubbles dominate the spectroscopic radiography (no absorption line), while the bright (but smaller-sized) spikes are detected in emission but not resolved in absorption.

Simulations indicate that targets driven by either the square or ramp pulse have traveled ~50 μm when the heat front has penetrated 5 μm of CH. Thus, in the absence of any stabilizing mechanisms, both pulses should experience similar RT growth. Targets irradiated by these two pulse shapes behave differently because the square pulse produces a shock that heats the target

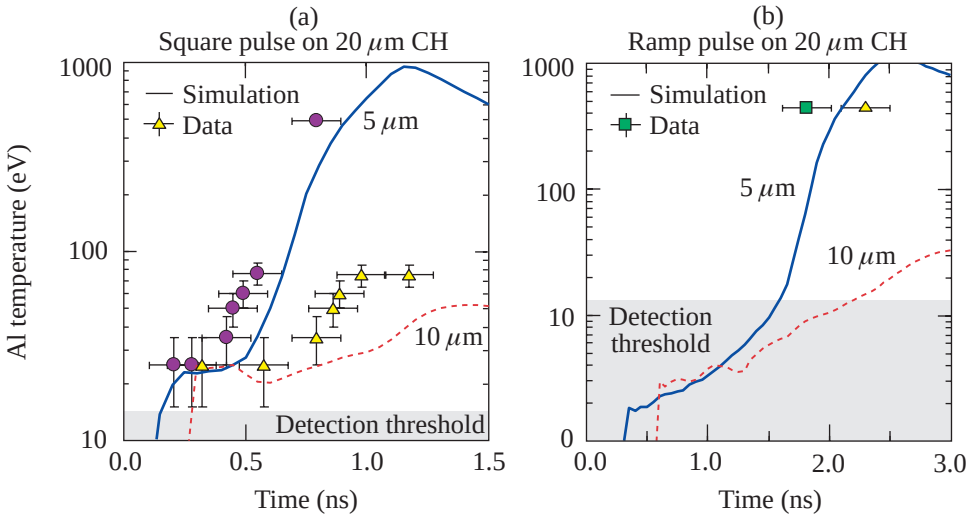

E10476, E10477

Figure 85.8
Comparison of the temperatures of the embedded Al layer as predicted by the 1-D code *LILAC* (curves) for various experiments and experimental data (points). (a) Square pulse driving the 5-μm case (solid/circles) and the 10-μm case (dashed/triangles). (b) Ramp pulse driving the 5-μm case (solid/circles) and the 10-μm case (dashed/triangles). Ramp-pulse data were present only for emission lines.

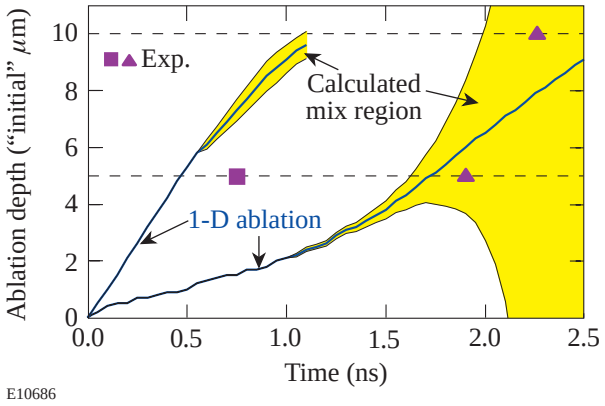

Figure 85.9
The ablation depths in uncompressed CH thickness. The heavy lines are the 1-D simulations, and the shaded regions are the calculated thickness of RT mixing. The measured penetration times are plotted at the embedded layer depths for the experiments.

to ~25 eV, causing it to decompress, thereby increasing the ablation velocity. This lowers the RT growth rate compared to that of the ramp pulse, which experiences less shock heating (<15 eV) and therefore little ablative stabilization. The simulations (which correctly model the observed shock temperatures) confirm that the square pulse produces ablation velocities that are as much as five times larger than those for the ramp pulse.

It has been shown that for the square-pulse drive, 1-D simulations accurately predict the observed shock heating (~25 eV) produced by an ~35-Mb shock and the heat-front penetration depth. In contrast, the ramp pulses produce ~15-Mb shocks that do not appreciably heat the target (<15 eV). The targets exhibit apparent anomalous heat-front penetration that results from two-dimensional effects caused by the RT instability.[15] Simulations of these experiments indicate that the shock heating produced by rapidly rising pulses causes the target to decompress, creating higher ablation velocities that reduce the RT growth rates. In contrast, the slowly rising pulse causes considerably less shock heating, producing less ablative stabilization, and therefore experiences significant effects due to the RT instability. This confirms the expected effect of shock heating and ablative stabilization on the stability of directly driven ICF targets.

ACKNOWLEDGMENT

This work was supported by the U.S. Department of Energy Office of Inertial Confinement Fusion under Cooperative Agreement No. DE-FC03-92SF19460, the University of Rochester, and the New York State Energy Research and Development Authority. The support of DOE does not constitute an endorsement by DOE of the views expressed in this article.

REFERENCES

1. J. D. Lindl, Phys. Plasmas **2**, 3933 (1995).
2. S. E. Bodner, D. G. Colombant, J. H. Gardner, R. H. Lehmberg, S. P. Obenschain, L. Phillips, A. J. Schmitt, J. D. Sethian, R. L. McCrory, W. Seka, C. P. Verdon, J. P. Knauer, B. B. Afeyan, and H. T. Powell, Phys. Plasmas **5**, 1901 (1998).
3. J. D. Kilkenny, S. G. Glendinning, S. W. Haan, B. A. Hammel, J. D. Lindl, D. Munro, B. A. Remington, S. V. Weber, J. P. Knauer, and C. P. Verdon, Phys. Plasmas **1**, 1379 (1994).
4. H. Takabe, L. Montierth, and R. L. Morse, Phys. Fluids **26**, 2299 (1983).
5. R. Betti, V. N. Goncharov, R. L. McCrory, P. Sorotokin, and C. P. Verdon, Phys. Plasmas **3**, 2122 (1996).
6. D. K. Bradley, J. A. Delettrez, and C. P. Verdon, Phys. Rev. Lett. **68**, 2774 (1992).
7. T. R. Boehly, V. N. Goncharov, O. Gotchev, J. P. Knauer, D. D. Meyerhofer, D. Oron, S. P. Regan, Y. Srebro, W. Seka, D. Shvarts, S. Skupsky, and V. A. Smalyuk, "The Effect of Plasma Formation Rate and Beam Smoothing on Laser Imprinting," submitted to Physical Review Letters.
8. T. R. Boehly, D. L. Brown, R. S. Craxton, R. L. Keck, J. P. Knauer, J. H. Kelly, T. J. Kessler, S. A. Kumpan, S. J. Loucks, S. A. Letzring, F. J. Marshall, R. L. McCrory, S. F. B. Morse, W. Seka, J. M. Soures, and C. P. Verdon, Opt. Commun. **133**, 495 (1997).
9. S. Skupsky and R. S. Craxton, Phys. Plasmas **6**, 2157 (1999).
10. C. Chenais-Popovics *et al.*, Phys. Rev. A **42**, 4788 (1990).
11. T. S. Perry *et al.*, J. Quant. Spectrosc. Radiat. Transf. **51**, 273 (1994).
12. D. Hoarty *et al.*, Phys. Rev. Lett. **82**, 3070 (1999).
13. D. Hoarty *et al.*, Phys. Rev. Lett. **78**, 3322 (1997).
14. M. C. Richardson, P. W. McKenty, F. J. Marshall, C. P. Verdon, J. M. Soures, R. L. McCrory, O. Barnouin, R. S. Craxton, J. Delettrez, R. L. Hutchison, P. A. Jaanimagi, R. Keck, T. Kessler, H. Kim, S. A. Letzring, D. M. Roback, W. Seka, S. Skupsky, B. Yaakobi, S. M. Lane, and S. Prussin, in *Laser Interaction and Related Plasma Phenomena*, edited by H. Hora and G. H. Miley (Plenum Publishing, New York, 1986), Vol. 7, pp. 421–448.
15. J. Delettrez, D. K. Bradley, and C. P. Verdon, Phys. Plasmas **1**, 2342 (1994).
16. R. Betti, V. N. Goncharov, R. L. McCrory, and C. P. Verdon, Phys. Plasmas **5**, 1446 (1998).
17. S. W. Haan, Phys. Rev. A **39**, 5812 (1989).
18. J. A. Delettrez, S. P. Regan, P. B. Radha, and R. P. J. Town, Bull. Am. Phys. Soc. **45**, 224 (2000).